Colloidal dispersions of cobalt ferrite nanoparticles in EMIM TFSI, propylene carbonate and their mixtures

A.A.A. Meireles Guerra, G. Gomide, S. Ibrahim, P. Burckel, P. Coppola, J. Depeyrot, R. Perzynski, V. Peyre, S. Papović, M. Vraneš, et al.

Colloids and Surfaces A: Physicochemical and Engineering Aspects 703 (2024) 135233

Contents lists available at ScienceDirect

Colloids and Surfaces A: Physicochemical and Engineering Aspects

journal homepage: www.elsevier.com/locate/colsurfa

Colloidal dispersions of cobalt ferrite nanoparticles in EMIM TFSI, propylene carbonate and their mixtures

A.A.A. Meireles Guerra [a,b,c], G. Gomide [c,d], S. Ibrahim [c], P. Burckel [f], P. Coppola [b], J. Depeyrot [d,e], R. Perzynski [c], V. Peyre [c], S. Papović [g], M. Vraneš [g], E. Dubois [c,*], A.F.C. Campos [a,b,c,e]

[a] Institute of Chemistry, University of Brasília, Brasilia, 70910-900, Brazil
[b] Laboratory for Environmental and Applied Nanoscience, University of Brasília, Planaltina Campus, Brasília, 73345-010, Brazil
[c] Sorbonne Université UMR CNRS 8234, PHENIX, 4 place Jussieu, case 51, Paris, 75005, France
[d] Complex Fluids Group, Institute of Physics, University of Brasília, Brasília, 70919-970, Brazil
[e] International Physics Center, Institute of Physics, University of Brasília, Brasília, 70910-900, Brazil
[f] Institut de Physique du Globe de Paris, 1 rue Jussieu, Paris, 75005, France
[g] Faculty of Sciences, Department of Chemistry, Biochemistry and Environmental Protection, University of Novi Sad, Trg Dositeja Obradovića 3, Novi Sad, 21000, Serbia

GRAPHICAL ABSTRACT

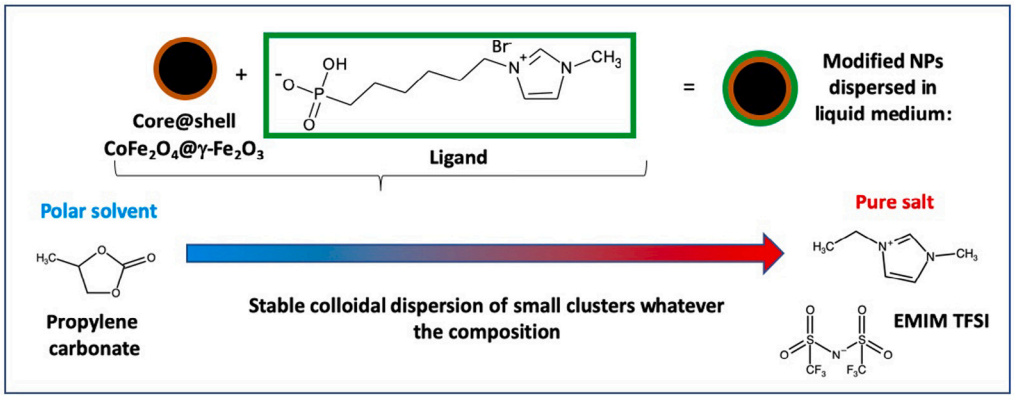

HIGHLIGHTS

- Magnetic cobalt ferrite NPs are dispersed as small clusters in EMIM TFSI up to 150 °C.
- The NPs are dispersed as small clusters in the polar solvent propylene carbonate.
- The NPs are stable in the mixtures of these solvents.
- Solvent removal by pumping followed by solvent addition highly reduces clustering.

ARTICLE INFO

Keywords:
Colloidal dispersion
Magnetic nanoparticles
Ionic liquid

ABSTRACT

Liquid thermocells are promising devices for the recovery of low-grade waste heat and its conversion into electricity. The present study proposes dispersing charged magnetic nanoparticles in liquids to improve thermoelectric conversion, due to their thermodiffusive and magnetic properties. Core@shell cobalt ferrite@maghemite nanoparticles (NPs) of various sizes with three different kinds of coatings are tested for

* Corresponding author.
E-mail addresses: anaaliceeq@gmail.com (A.A.A.M. Guerra), emmanuelle.dubois@sorbonne-universite.fr (E. Dubois), relex@unb.br (A.F.C. Campos).

https://doi.org/10.1016/j.colsurfa.2024.135233
Received 10 July 2024; Received in revised form 20 August 2024; Accepted 30 August 2024
Available online 10 September 2024

Concentrated electrolytes
EMIM TFSI
Propylene carbonate

dispersion in EMIM TFSI (ethyl-methylimidazolium bistriflimide), an ionic liquid (IL) of high electrical conductivity. Among the tested ligands, $PAC_6MIM^{\pm}Br^{-}$ (1-(6-hexylphosphonate) 3-methyl imidazolium bromide) emerges as the most efficient due to its phosphonic group. This ligand leads to dispersions of clusters of a few dozen NPs in water and a few NPs in EMIM TFSI. For improving both the viscosity and the electrical conductivity, dispersions in binary mixtures of propylene carbonate (PC), a polar medium, and EMIM-TFSI are further investigated with the sample based on NPs of ~ 9 nm diameter. Through a pumping and heating procedure, stable dispersions are obtained with a subsequent reduction of the size of the NP clusters, down to 1 to 2 NPs in EMIM TFSI and a few NPs in PC and their binary mixtures. The mixture with an IL mole fraction ~ 0.2–0.3 and maximal electrical conductivity is a promising candidate for further thermoelectric investigations.

1. Introduction

Given the always increasing global energy demands and environmental deterioration, the development of new solutions for sustainable energy is mandatory. Considering this scenario, the use of thermoelectric devices for the conversion of low-grade waste heat [1] into electricity may be an interesting option [2]. However, its contribution is relatively small compared to other sustainable sources due to the low efficiency of converting heat into electricity, highlighting the need for further investigation into new materials.

In this context, colloidal dispersions of charged nanoparticles (NPs) are particularly notable, as both the NPs and the solvent can exhibit promising characteristics for thermoelectric applications [3,4]. The thermoelectric efficiency in these systems is particularly connected to the thermodiffusion of the charged species. Among these dispersions, ferrofluids stand out (see [5] and Refs. therein) due to their thermodiffusive and their magnetic properties, which offer the potential for enhancing thermoelectric efficiency by exploiting these characteristics [6]. A study demonstrated that incorporating iron oxide NPs into an aqueous dispersion improved thermoelectric efficiency by approximately 30% [7].

Regarding the contribution of the solvent, it is preferable to choose those capable of withstanding high temperatures, as this can improve the efficiency of thermoelectric conversion [8–10]. Two promising candidates are ionic liquids (ILs) and propylene carbonate (PC), each representing opposite ends of the ionic character spectrum. ILs boast higher conductivity as they consist solely of ions. However, they tend to be more viscous than traditional solvents, which could pose challenges to the electrochemical conversion process. Among ILs, EMIM TFSI (ethyl-methylimidazolium bistriflimide) is especially attractive for thermoelectric applications due to its good sensitivity to electric fields [11], high thermal stability, and lower viscosity compared to other ILs [12]. On the other hand, PC offers much lower viscosity but has a non-ionic nature. Considering this, mixtures of IL and PC could serve as a viable solution, achieving a balance between viscosity and electrical conductivity to enhance performance. Indeed, hybrid ionic liquid propylene carbonate-based electrolytes have been developed to efficiently replace classical organic solvents in batteries and supercapacitors [13,14].

In previous studies, stable colloidal dispersions of maghemite NPs in pure ILs [15,16] and mixtures of the IL ethylammonium nitrate and water [17] were obtained by precisely controlling the NPs/solvent interface. Parameters such as the nature of the IL ions and the state of the NPs surface (especially charge, and nature of ligand and counterion) were found to be crucial for achieving stable colloidal dispersions. This work aims to take a step further and investigate core@shell nanoparticles with a cobalt ferrite core and a maghemite-rich shell. These particles are particularly interesting because their core exhibits much higher magnetic anisotropy, which can enhance thermoelectric efficiency, as suggested by some modeling and simulation studies [18,19]. Moreover, their shell provides long-term chemical stability and high surface tunability, with a composition similar to that of previously studied NPs.

Thus, this study seeks to assess the impact of several parameters on colloidal dispersions of core@shell magnetic NPs ($CoFe_2O_4$@γ-Fe_2O_3), including NP composition and size, and the nature of the ligand used to adjust the NP surface. These dispersions are examined in both pure EMIM TFSI and PC, as well as their mixtures across different mole fractions. Additionally, the effect of heating during NP surface functionalization is investigated to determine its influence on ligand adsorption and NP leaching. Various characterization techniques such as X-ray diffraction (XRD), transmission electron microscopy (TEM), magnetic measurements, Dynamic Light Scattering (DLS), and Small-Angle X-ray Scattering (SAXS) are employed to evaluate colloidal dispersion stability, with a specific focus on their potential for thermoelectric applications.

2. Components

2.1. Nanoparticles

2.1.1. Synthesis

Initial samples of water-based ferrofluids containing $CoFe_2O_4$@γ-Fe_2O_3 NPs of three different mean sizes were synthesized through a well-established procedure [20], which can be divided into three main steps. First, the cobalt ferrite core is synthesized by coprecipitation in an alkaline medium. The NPs mean size can be roughly tuned by the strength of the base used in this stage. As a general trend, the stronger the base, the larger the mean size, while keeping the other synthesis parameters constant [21]. The second step involves the formation of the maghemite shell through a hydrothermal treatment with $Fe(NO_3)_3$ solution. Finally, in step three, the NPs are peptized in water at pH ≈ 2, where they bear a positive structural surface charge of approximately 2 charges per nm^2 [22]. Here, ammonium hydroxide (NH_4OH), methylamine (CH_3NH_2) and sodium hydroxide (NaOH) were used as bases in the coprecipitation route to produce samples of increasing average sizes, labeled as APCo1, APCo2, and APCo3, respectively. The details of the experimental conditions of the synthesis are described in Section 1 of the Electronic Supporting Information (ESI).

2.1.2. Characterization techniques

The crystalline structure of the NPs was examined using XRD. The diffractograms were compared with standard reference patterns for cobalt ferrite and maghemite, and the average diameter d_{XR} of the crystallites was calculated using the Scherrer equation.

The shape and size of the NPs were analyzed through TEM. Particle sizes were measured using an image processing software, and the resulting size distribution histograms were fitted with a log-normal distribution function to determine a median size d_0 and a polydispersity index s.

To analyze the chemical composition of the NPs, flame atomic absorption spectroscopy (FAAS) was used to measure iron and cobalt concentrations (see ESI section 2.3). The proportion of the maghemite shell was determined considering a core@shell model of composition, *i.e.* a core of cobalt ferrite surrounded by an iron oxide shell [20].

Magnetization measurements were recorded with a SQUID magnetometer on dispersions of NPs coated with $PAC_6MIM^{\pm}Br^{-}$ ligands (see Section 3.1) in water around 1 vol% of NPs at room temperature (see ESI section 2.4. for details). The average magnetization of the NPs is determined from the extrapolation at infinite magnetic field at high fields. μ_o being the permeability of vacuum, the dipolar parameter $\Psi_{dd} = \mu_o m_s^2 \pi d^3/6kT$ of NPs of diameter d is determined from the

Table 1
NP's characteristics : Cell parameter ($\langle a \rangle$) and mean characteristic diameter (d_{XR}) deduced from XRD experiments; Median diameter d_0 and polydispersity index (s) deduced from TEM determinations; Fraction of maghemite shell ($\frac{\Phi_S}{\Phi_{NP}}$) deduced from FAAS measurements and thickness e of the shell; saturation magnetization m_s of the NPs and dipolar parameter Ψ_{dd} (see text for details).

Sample	$\langle a \rangle$ (nm)	d_{XR} (nm)	d_0 (nm)	s	$\frac{\Phi_S}{\Phi_{NP}}$	e (nm)	m_s (kA/m)	m_s (Am^2/kg)	Ψ_{dd}
APCo1	0.826	4.0	4.1	0.33	0.56	0.44	82	15.8	0.58
APCo2	0.830	7.4	8.9	0.28	0.28	0.35	229	43.3	12
APCo3	0.832	13.4	11.9	0.35	0.15	0.31	323	60.5	70

initial susceptibility χ, *i.e.* the linear part of the low field magnetization (< 800 A/m = 100 Oe), by $\Psi_{dd} = 3\chi/\Phi$. For individually dispersed objects (NPs or clusters), the dipolar interaction parameter Ψ_{dd} is then a characteristic of their size distribution and the value Ψ_{dd} reveals their capacity to form chains ($\Psi_{dd} >> 8\pi$) or not ($\Psi_{dd} << 8\pi$) due to dipolar magnetic interactions [23].

2.1.3. Characterization results

Regarding the X-ray diffractograms (see Section 2.1 of the ESI), the identified pattern corresponds to a spinel structure for all the three samples. This observation is supported by the derived lattice parameter values < a > presented in Table 1. The mean diameter d_{XR} (given in Table 1) is deduced from the peak broadening for the three samples. Notably, the three very different mean sizes obtained here show that the selected approach to control size proves to be successful.

The size distribution histograms derived from processing the TEM images can be satisfactorily fitted with a log-normal distribution (see Section 2.2 of the ESI). The median diameter d_0 and the polysispersity index s deduced from this fitting are presented in Table 1.[1]

In the framework of the core@shell model, the fraction of maghemite shell is deduced from FAAS measurements. They are presented in Table 1, where Φ_S and Φ_{NP} are respectively the volume fraction of the maghemite shell and of whole NP. As it can be seen in Table 1, the fraction of the shell decreases as the NPs size increases. This result can be attributed to the material's nanoscale characteristics, wherein the surface-to-volume ratio is larger for smaller particles. The corresponding thickness of the shell is of the order of the lattice size of the spinel oxide.

Both the saturation magnetization of the NPs m_s and the parameter Ψ_{dd} are given in Table 1. This latter characterizes NPs for APCo1 as the magnetic interaction between NPs at contact is negligible in front of kT. It represents an effective value of the dispersed clusters (discussed later in the text) for APCo2 and APCo3 for which these interactions are respectively close to kT and larger than kT. The huge difference in magnetic properties due to the size of the NPs nevertheless clearly appears. No chains are expected in APCo1 and APCo2, whereas chaining of the bigger particles is expected in APCo3 as $\Psi_{dd} >> 8\pi$ [23].

In conclusion, all the techniques point towards huge differences of properties between the three synthesis APCo1, APCo2 and APCo3.

2.2. Solvents

In addition to its specific role in the colloidal stabilization of the NPs, the solvent composition can be chosen for its properties in regard to a specific application. For thermoelectric uses, high temperature stability, not too large viscosity and high electrical conductivity are required. In this study, the magnetic core@shell nanoparticles are dispersed in EMIM TFSI, a well-known ionic liquid used in a recent work with different NPs [24], PC, and also in their binary mixtures. PC is an interesting polar solvent used in batteries that boils at 242 °C with a low viscosity of 2.5 mPa s at 20 °C and a dielectric constant of 64. Thus, a systematic characterization of the viscosity and electrical conductivity of these solvents as a function of temperature and composition is carried out. The goal was to find the optimal solvent composition aiming for a good compromise between low viscosity and high electrical conductivity to improve the thermoelectric properties of the final colloid. The experimental details of procedures and equipment used for the physico-chemical measurements are described in Section 3 of the ESI.

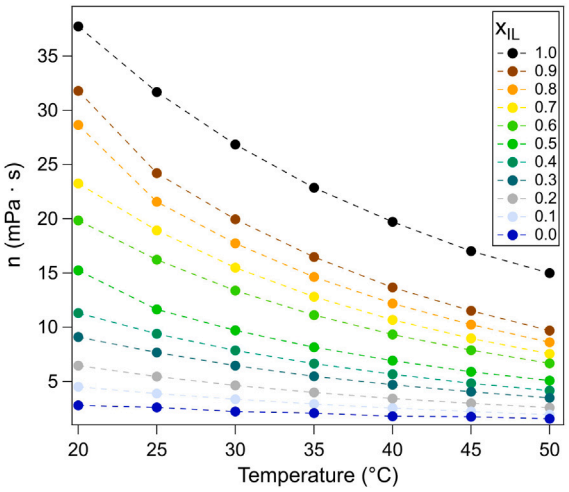

Fig. 1. Viscosity of the EMIM TFSI + PC mixtures as a function of temperature for different EMIM TFSI mole fractions (x_{IL}).

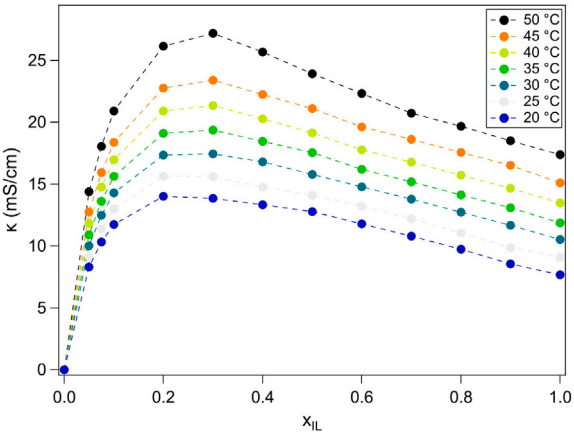

Fig. 2. Electrical conductivity of the EMIM TFSI + PC mixtures as a function of EMIM TFSI mole fraction (x_{IL}) at different temperatures.

Fig. 1 exhibits the impact of IL proportion on the viscosity of the binary mixture as a function of temperature (20 to 50 °C) for different EMIM TFSI mole fractions (x_{IL}). As expected, the viscosity decreases with increasing temperature since the thermal energy makes the molecules more mobile. The viscosity also reduces with increasing PC amount, which is consistent with the disturbance of the ordered structure of the IL by the PC molecules that insert themselves between the IL ions [14,25].

[1] Note that the polydispersity index s obtained by TEM is always lower than with other techniques because TEM fails to capture the full distribution of sizes due to the aggregation induced by the sample's preparation

The electrical conductivity of the binary mixture is shown in Fig. 2 as a function of mole fraction x_{IL}, at various temperatures from 20 °C up to 50 °C. The addition of PC progressively reduces x_{IL} and first steadily increases the electrical conductivity of the system, down to x_{IL} values between 0.2–0.3, regardless the temperature in the whole experimental range. This behavior arises from the effective solvation of EMIM TFSI ions by PC molecules. The IL ions become gradually more loosened because some of the cation–anion interactions are replaced by strong H-bonds between the $EMIM^+$ cations and PC [26,27]. Conversely, decreasing x_{IL} below 0.2–0.3, the electrical conductivity of the binary mixture sharply decreases down to zero, due to the non-ionic character of the PC solvent. This maximum of the conductivity around x_{IL} = 0.25 (50 °C) corresponds to a composition of 3 PC molecules for 1 EMIM TFSI, and in other units to a volume fraction of IL around 0.5 or a concentration of EMIM TFSI around 2 mol/L.

3. Solid/solvent interface

3.1. Choice of the ligand

Several surface ligands are tested to adjust the NPs' surface prior to their transfer into the IL, through a wet route proposed by Riedl et al. in [24][2]. In this process, the nitrate counter-ions, which compensate for the positive surface charge of the NPs in the synthesized aqueous ferrofluids, are replaced with imidazolium-based ligands (see below and Section 4 of the ESI). For this, NaOH solution of 0.1 mol/L is gradually added until reaching the point of zero charge of the nanoparticles (pH ≈ 7), which are then magnetically separated and washed several times with ultrapure water to remove all ions. Following this, the ligands in their acidic form are added until a pH of approximately 2 is reached (with a ligand concentration ≈ 75 mmol/L). If the ligand is appropriate, the NPs are redispersed. To transfer the coated NPs in the pure IL, equivalent volumes of NP dispersion in water and of pure EMIM TFSI are mixed, the water being further removed by pumping at 0.0031 mbar for 24 h at room temperature

The colloidal stability of the final sample in EMIM TFSI is assessed by comparing the hydrodynamic diameters (d_H) acquired from DLS measurements. More details about the equipment and experimental conditions are described in Section 2.5 of the ESI.

Three different ligands (see the drawn molecules in Section 4 of the ESI) are tested here:

(i) $SBMIM^{\pm}TFSI^-$ (1-(4-butylsulfonate)-3-methyl imidazolium bistriflimide), from Solvionic, France
(ii) $PAC_6MIM^{\pm}Br^-$ (1-(6-hexylphosphonate) 3-methyl imidazolium bromide), from Sikemia, France
(iii) $PAC_4MIM^{\pm}Br^-$ (1-(6-butylphosphonate) 3-methyl imidazolium bromide), from Sikemia, France, special synthesis on demand

This choice of ligands allows to sort out both the importance of the nature of the negative group adsorbing on the NPs and the influence of the side-chain length. Indeed the first ligand adsorbs on the positively charged NP surface via its negative sulfonic group, while the two others adsorb via their negative phosphonic group. Therefore, the first and the third ligand only differ by the negative charged group, as they have the same butyl side-chain. On the contrary the second and the third differ by the side-chain length, keeping the same phosphonic negative group.

Although $SBMIM^{\pm}TFSI^-$ was successfully used with maghemite NPs in [24], it here fails to stabilize the present cobalt ferrite NPs in EMIM TFSI, whatever their size. However, $PAC_6MIM^{\pm}Br^-$ produces stable dispersions in EMIM TFSI. As the two ligands differ by both their negative group that adsorbs on the NPs (phosphonic or sulfonic) and their side-chain length, $PAC_4MIM^{\pm}Br^-$ is tested in order to identify the origin of the difference. As the dispersion of NPs is also achieved with this shorter side chain similar to the one of the $SBMIM^{\pm}$ zwitterion, we conclude that the difference comes from the nature of the group that attaches on the NPs' surface. Note that such phosphonic ligands also enable titrations of atoms that are not present in the solvent so that the amount of molecules around the NPs can be studied.

[2] Note that the initial aqueous dispersions in nitric acid are not stable in EMIM TFSI

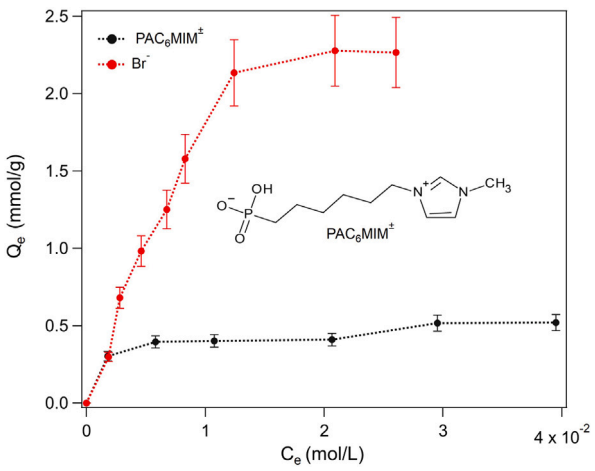

Fig. 3. Adsorption isotherms of $PAC_6MIM^{\pm}$ and Br^- onto the APCo2 NPs dispersed in water (coating realized at 80 °C). For the definition of adsorbed Q_e and free C_e, see Section 5 of the ESI.

3.2. Isotherms with $PAC_6MIM^{\pm}Br^-$ in water

Because of the successful outcomes [24] previously achieved with dispersions of maghemite NPs of diameter 8.7 nm, similar to those of the present APCo2 sample, the adsorption isotherm determinations are conducted only with the APCo2 sample. Moreover, taking into account the previous tests on the ligands, the functionalization of the APCo2 NPs by $PAC_6MIM^{\pm}Br^-$ in water was chosen to evaluate the coating stability, the adsorption capacity, and the effect of temperature on the process. The experimental conditions are adapted from Djaniš et al. [28]. To assess the influence of temperature, another adsorption test without heating was conducted using a sample prepared following the conditions of Riedl et al. [24], at room temperature. The details of all adsorption experiments are described in Section 5 of the ESI.

The equilibrium adsorption isotherms of $PAC_6MIM^{\pm}$ and Br^- onto the APCo2 NPs are depicted in Fig. 3. The surface coating at 80 °C reaches a saturation regime at high concentrations, indicating a limit adsorption capacity of approximately 0.5 mmol/g for $PAC_6MIM^{\pm}$ and 2.25 mmol/g for Br^-. Considering the NPs as isolated hard spheres, this surface coverage corresponds to ≈ 2.3 $PAC_6MIM^{\pm}/nm^2$ and ≈ 10.5 Br^-/nm^2.

Regarding the unheated sample, one found a surface coverage of ≈ 1.7 $PAC_6MIM^{\pm}/nm^2$, indicating that the temperature has a minor impact on the $PAC_6MIM^{\pm}$ adsorption within the investigated range. However, in the case of Br^-, the coating reduced to ≈ 1.1 Br^-/nm^2, without heating. This behavior may be attributed to the tendency of bromide ions to primarily form outer-sphere complexes with oxide surfaces, rendering the adsorption process more sensitive to temperature variation [29].

The functionalization of iron oxide-based NPs with phosphonic ligands in acidic media can partially dissolve the particle surface. It mainly arises from the strong chemical interaction between the surface iron ions with phosphonate groups [30], a process that can be affected by the temperature of the coating process. Here, the results of the leaching tests are reported in Section 5 of the ESI (Fig. S11), where the mass fraction of leached iron and cobalt ions is plotted as a function of the initial PAC_6MIMBr concentration for heated and unheated samples.

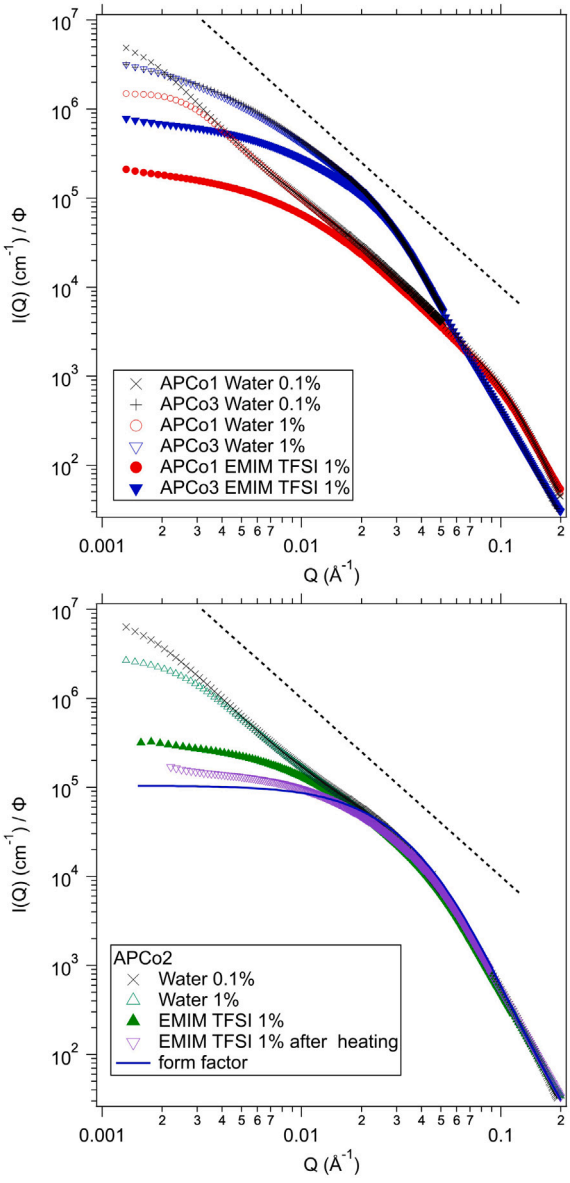

Fig. 4. Scattered intensity I(Q) in absolute scale normalized by the volume fraction of NPs, Φ_{NP}, for the three sizes of NPs with $PAC_6MIM^{\pm}$ ligands on their surface (all rescaled with the contrast of water). APCo1 and APCo3 are in the top graph, APCo2 is on the bottom graph. Black crosses: water samples at Φ_{NP} = 0.1%, empty symbols: water samples at Φ_{NP} = 1%, full symbols: EMIM TFSI samples at Φ_{NP} = 1%. Dotted lines have a slope 2 marking an intermediate fractal dimension for the clusters in water of APCo1 and APCo2 samples. For APCo2, a possible form factor calculated with a lognormal distribution of spheres and based on the large Q's region is added on the graph (d_0 = 5 nm and σ = 0.45).

The leaching of cobalt is much lower than that of iron for all samples, which may be attributed to the iron-rich external layer of the nanoparticles. Concerning the impact of temperature, one can analyze the iron leaching in both heated and unheated samples with the same ratios of PAC_6MIMBr concentration and nanoparticle mass (highlighted points). The results show that the NPs coated at 80 °C leak approximately 3 times more iron than those at room temperature.

From the previous results, the coating of the NPs at higher temperatures increases leaching and does not significantly affect the surface coverage with $PAC_6MIM^{\pm}$. Thus, in further experiments involving the elaboration of samples in EMIM TFSI, PC and their binary mixtures, the functionalization of the NPs was carried out at room temperature.

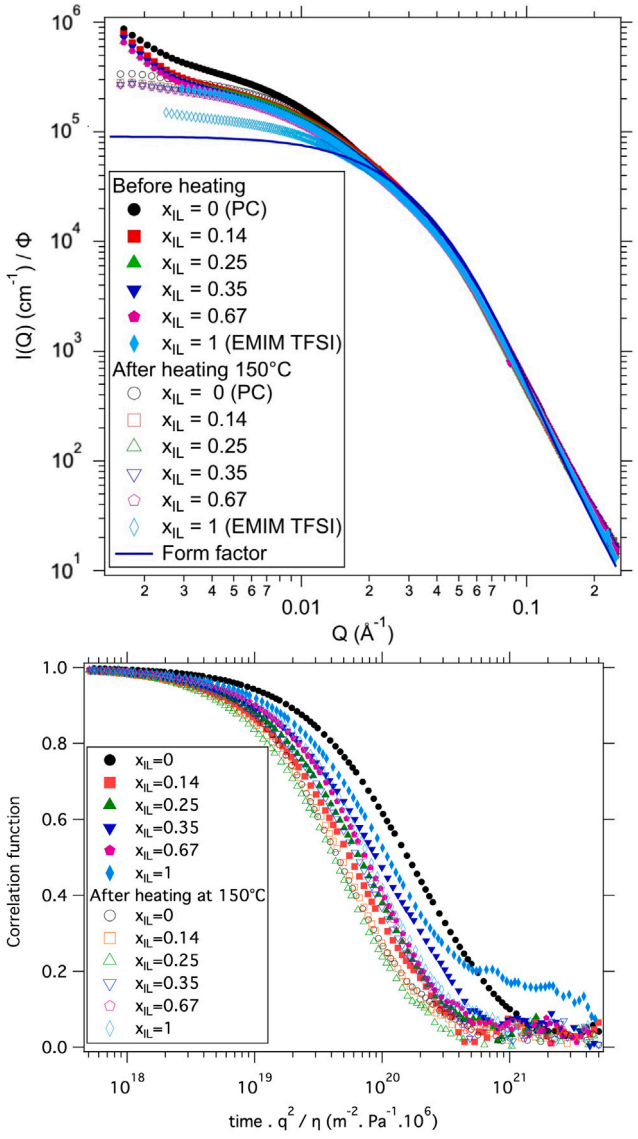

Fig. 5. Top: Scattered intensity I(Q) from SAXS, in absolute scale rescaled with the contrast of propylene carbonate (PC) for all samples in the EMIM TFSI/PC mixtures, before and after heating, for Φ_{NP} = 1% (APCo2). x_{IL} is the mole fraction of ionic liquid in the mixture. The symbols are given in the legend (see Fig. S10 in ESI for a zoom on small Qs). Bottom: DLS of the same samples, with a rescaled X-axis in order to compare the different solvents removing the effect of the variation of refractive index and viscosity.

4. Dispersions of NPs coated with $PAC_6MIM^{\pm}$ in different solvents

The dispersions of $PAC_6MIM^{\pm}$-coated NPs in the different solvents are studied in detail to assess the quality of the dispersions, their ageing, and the interaction between the dispersed objects. After a first evaluation of the dispersions by DLS as above, SAXS is performed to get a more precise information on the nanoscale ordering (See section 2.6 in ESI for details). Nanoparticles from the APCo2 sample were dispersed in all tested solvents and mixtures, whereas NPs from the APCo1 and APCo3 samples were dispersed only in water and pure EMIM TFSI.

4.1. Dispersions in acidic water

The NPs coated with $PAC_6MIM^{\pm}$ are dispersed in water at pH ≈ 2 and hold a positive charge. DLS shows clusters, the smaller are the NPs, the larger are the clusters (see Table 2). The radius of gyration R_g

determined from the SAXS measurements on the most dilute sample (Φ_{NP} = 0.1%) leads to the same conclusion.

Clusters, like the present ones with a fractal dimension of the order of 2 (see Fig. 4), have been observed in aqueous dispersions rather similar to APCo1 and APCo2 while varying the pH and salt concentration [31]. Those clusters were issued from Reaction Limited Colloidal Aggregation (RLCA) [32] which is a universal process, independent of the detailed chemical nature of the colloidal system.

In APCo3, the NPs are much bigger and are able to produce chains and loops due to the large value of the dipolar magnetic interaction parameter [33], leading to a very different situation.

However here, no conditions can be reached to directly obtain the form factor of the dispersed NPs. A possible form factor for APCo2 is plotted in Fig. 4 bottom, based on the intensities at large Q's. The comparison of the intensities at low Q's for the most dilute sample and this form factor gives an approximate number of aggregation N_{agg} of 40 to 50.

From Fig. 3-left of the previous study [31], a N_{agg} can also be evaluated using the present measurements of R_g. The estimated values of N_{agg}, given in Table 2, also show clusters of a few dozen of NPs.

The series of 4 concentrations measured (0.1 to 3 vol%, diluted keeping the ligand concentration constant) show that there is a repulsion between these clusters, stronger for smaller NPs. (see Fig. 4 and Fig. S7). This is consistent with the long-term stability of these dispersions of clusters.

4.2. Dispersions in pure ionic liquid EMIM TFSI

The samples are produced according to the process described in Section 3.1. The final volume fraction in the IL is thus known as well as the concentrations of all the introduced species.

In order to assess the coating stability post-transfer to the IL, the amounts of $PAC_6MIM^{\pm}$ and Br^- were determined around the NPs after ultracentrifugation for APCo2, resulting in 0.52 and 0.06 mmol/g, respectively (see experimental details in Section 5 of the ESI). This surface coverage corresponds to ≈ 2.4 $PAC_6MIM^{\pm}/nm^2$ and ≈ 0.3 Br^-/nm^2, which is very close to the limit adsorption capacity for $PAC_6MIM^{\pm}$ in water, but much lower for Br^-, which seems to desorb from the solid/liquid interface in the IL. These results indicate that the coating with $PAC_6MIM^{\pm}$ is robust and improves in EMIM TFSI medium.

After the transfer to the IL, the size of the clusters is all the more reduced as the individual NPs are smaller, according to both DLS and SAXS (Table 2 and Fig. 4). Moreover the sizes of the dispersed entities are very close for the different samples, both from DLS and SAXS.

From a series of volume fractions, the interobjects interactions appear very weak (see Fig. S8). Note that APCo3 dispersions are not fully stable at Φ_{NP} = 1%, with a small precipitate appearing with time. This is consistent with previous studies that showed the difficulty of stabilizing larger particles at large concentrations [34].

Heating the sample APCo2 at 150 °C during 2 h[3] reduces further the R_g from 26 nm to 13 nm (see Fig. 4 bottom). Finally, according to SAXS measurements, the sample is stable for one year at least, with a N_{agg} of the order of 1 to 2.

4.3. Dispersions in propylene carbonate (PC)

The samples in pure PC cannot be prepared in the same way as the IL-based ones because PC vaporizes while pumping. Moreover, heating a PC/water mixture with the NPs destroys the solvent, that becomes very viscous. This probably results from the opening of the carbon ring as observed in this family of molecules [35], here enhanced by the presence of oxide NPs. The only possible path was therefore to try an intermediate powder state. Water is first removed from an aqueous dispersion of NPs coated with $PAC_6MIM^{\pm}$ (see Section 4.1) by pumping (0.0031 mbar, 24 h, room temperature) before adding PC. Visual redispersion of the NPs is obtained after heating few minutes at 80 °C.

The scattered intensity for APCo2 is plotted in Fig. 5 and evidences some aggregation at low Q's. Heating 2 h at 150 °C destroys these clusters and leads to an apparent R_g slightly larger but close to the value obtained in the pure EMIM TFSI after heating (see Table 3).

PC is a polar solvent with a dielectric constant of 64. Given the amount of adsorbed ligand molecules and the total number introduced, the free ligand concentration is around 0.05 mol/L and the NPs are positively charged with bromide counterions. It means that the electrostatic contribution effectively stabilizes the NPs in PC, with some steric contribution due to the size of the ligand.

4.4. Dispersions in mixtures of EMIM TFSI and PC

Several compositions EMIM TFSI/PC are chosen according to the conductivity measurements on the pure solvents, for which the maximal conductivity is obtained with mole fractions x_{IL} = 0.2 to 0.3 depending on the temperature (see Fig. 2).

In order to avoid drying the NPs by pumping, the mixtures are produced by adding PC in a concentrated dispersion in EMIM TFSI at Φ_{NP} = 3%.[4] A volume fraction Φ_{NP} = 1% is reached for several compositions: x_{IL} = 0.14, 0.25, 0.35 and 0.67. Whatever the value of x_{IL}, the samples look stable by eye and DLS confirms that the objects are rather small. Note that the rescaled SAXS scattered intensities are superimposed on large Q's, which shows that the individual NPs are not modified. Interestingly, adding PC in EMIM TFSI creates some clusters, evidenced by the low Q upturn, as in pure PC obtained with the dried NPs (see Fig. 5-top).

However, after 2 h of heating at 150 °C, the aggregation is reduced. In Fig. 5 bottom, the correlation functions from DLS are plotted as a function of $t \cdot Q^2/\eta$ where Q is the scattering vector and η the viscosity of the solvent. This allows removing the influence of the refractive index

Table 2
Sizes (in nm) obtained either from DLS (hydrodynamic diameter d_H) on Φ_{NP} = 1% dispersions or from SAXS (radius of gyration R_g) on Φ_{NP} = 0.1% dispersions. The particles are all coated with the $PAC_6MIM^{\pm}$, thus the particles in water appear positively charged with bromide counterions. The N_{agg} is deduced from R_g and Fig. 3-left of [31], both in water and in IL.

Solvent	Parameter	APCo1	APCo2	APCo3
Water	d_H (nm)	101	72	47
Water	R_g (nm)	61	55	36
Water	N_{agg}	~25	~20	
IL	d_H (nm)	59	50	45
IL	R_g (nm)	29	26	28
IL	N_{agg}	~4	~3	

Table 3
Sizes determined from the dispersions in the different solvents after heating at 150 °C (particles APCo2). The radius of gyration R_g is extracted from SAXS (Φ_{NP} = 0.1%) and the hydrodynamic diameter d_H is obtained from DLS (Φ_{NP} = 1%).

x_{IL}	R_g (nm)	d_H (nm)
0 (PC)	19	25
0.14	17	26
0.25	14	23
0.35	14	33
0.67	14	41
1 (EMIM TFSI)	13	43

[3] Heating in close vessels, thus not removing water.

[4] It is simply produced by adding $V_{EMIMTFSI} = V_{water}/3$ during the phase transfer instead of an equal volume (see Section 4.2). There is no heating step.

and of the viscosity, which differ in the different solvents. The shifts between the curves are thus only due to a difference in the apparent sizes of the objects. It evidences a decrease of the d_H when heating: the correlation functions with empty symbols are always on the left of the ones with full symbols, the higher shift occurring for pure PC. The tail of the correlation function for pure EMIM TFSI at long times, evidencing some bigger clusters, also disappears after heating. All these results are confirmed by SAXS (Fig. 5 top). As for the pure solvents, the heating step improves the dispersion state of the NPs, breaking some small clusters.

The comparison of SAXS intensities at 1 vol% of NPs and 0.1 vol% evidences a repulsive interaction between NPs, within the hypothesis that the clusters are not modified by dilution (see Fig. S10 in ESI). The apparent sizes extracted from DLS are equal to or lower than the value in the pure IL. The R_g, gathered in Table 3, decrease from pure PC to pure EMIM TFSI. This discrepancy between the two techniques cannot be explained solely by the interactions, therefore clusters may depend on the dilution, remaining however constituted of few NPs in the range explored.

5. Discussion

5.1. Influence of the ligands

The first surprising result is the impossibility to stabilize the cobalt ferrite NPs here with the SBMIM± ligand, regardless of their size. This is unexpected, as this ligand effectively stabilizes iron oxide NPs of similar size up to 200 °C and over extended periods [24]. Only the phosphonic based molecules stabilize these cobalt ferrite NPs. Note that they also stabilize the iron oxide ones [36], for which no major difference of behavior appears when moving from the sulfonic to the phosphonic anchoring group.

Another difference between the iron oxide and the cobalt ferrite NPs is the material of the core, as their surfaces are quite similar due to the same surface treatment applied at the end of the synthesis. The core@shell NPs are predominantly composed of cobalt ferrite since their iron-rich layer is very thin, less than the lattice parameter of the spinel structure (Table 1). This difference in composition can impact the interparticle attractive interactions. The Hamaker constant for cobalt ferrite ($\approx 4 \times 10^{-19}$ J) [37,38] is slightly higher than for maghemite ($\approx 2.3\times10^{-19}$ J) [39], resulting in stronger attractive van der Waals interaction. Moreover, cobalt ferrite NPs present higher magnetic anisotropy than maghemite for a similar NPs' diameter (see ESI for details, section 2.4., Fig. S6), which can enhance the contribution of the magnetic dipolar interactions inside the clusters, especially for the largest NPs. It remains however a small contribution compared with the van der Waals interaction. These factors may contribute to the main contrast behavior of the two types of NPs, observed in the initial aqueous acidic dispersions: there is indeed no aggregation with the iron oxide NPs dispersed in the media of similar compositions.

One important difference between the ligands is nevertheless the stronger interaction of the phosphonic group with the oxide surfaces compared with the sulfonic groups [30]. These authors showed that a ligand with both a sulfonic and a phosphonic group attaches with the phosphonic part on barium hexaferrite platelets due to a stronger interaction with the iron for this phosphonic group. This latter can attach on the oxides by different mechanisms depending on the material, pH, and reaction conditions [40], the bonding being covalent or partly covalent.

Finally, the phosphonic group/iron interaction is stronger than the sulfonic/iron one, which should improve the coverage of phosphonic molecules on the iron layer of the cobalt ferrite NPs. Phosphonic ligands may also better succeed to cover the NPs' surface despite the initial clusters, and also help to break them.

Table 4
Results from the Karl-Fisher titrations of the water extracted in a furnace at 150 °C. The raw solvents are those used for the preparation of the dispersions of Section 4. NPs are here APCo2 and the ligand is the $PAC_6MIM^{\pm}$. See text for details.

Sample	ppm	Weight %	vol %
Propylene carbonate (PC)	10	0.001	0.0012
EMIM TFSI (IL)	43	0.0043	0.0065
IL H_2O saturated	7500	0.75	1.13
IL H_2O saturated redried	744	0.074	0.112
NPs+ligand in IL (after pumping)	800	0.08	0.12
Dried (NPs+ligand) in PC	1800	0.23	0.27

5.2. Remaining water

Although EMIM TFSI is rather hydrophobic, it can dissolve some water while PC is much more hygroscopic [41]. Moreover, the process of preparing the samples raises questions about the water content at the end, an amount that can have a huge impact on the properties, especially at the solid/solvent interface [42]. Could it explain here the formation of clusters when adding PC in EMIM TFSI before heating?

The water has been determined by heating the sample at 150 °C in a furnace connected to a Karl Fisher electrochemical cell (Metrohm, see Section 2.7 of the ESI for details). Table 4 gathers the results that are given in ppm classically used, in weight percentage and also in volume percentage to be able to compare the different solvents getting rid of the differences in densities. The raw solvents are those used for the preparation of the dispersions of Section 4. The values obtained from the IL dispersions after pumping (0.0031 mbar) to remove the water are provided in the third part of the table. This process is applied to produce the colloidal dispersions in the IL EMIM TFSI, not in PC (see Section 4.3).

The original solvents are quite dry. However, EMIM TFSI takes 1.13 vol% of water after 24 h in contact with moisture, equivalent to 0.63 mol/L or 1 water molecule for 6 EMIM TFSI. When this mixture is pumped to remove the water (0.0031 mbar, 24 h, room temperature), the content decreases back only to 0.112 vol%, which corresponds to 1 water for around 60 EMIM TFSI. During particles transfer to the ionic liquid, EMIM TFSI is mixed with the acidic aqueous dispersion of coated NPs, followed by pumping. The final water content (0.12 vol%) is very close to this latter value, meaning that the water here comes from the solvent, and that the NPs do not retain much water.

On the contrary, when the particles are transferred to PC, they are first dried before adding PC solvent. In this case, the final water content is higher, and the water mostly comes from the NPs, as the PC is very dry.

The addition of PC to the concentrated EMIM TFSI-based colloidal dispersion decreases the water content because PC contains very little water. Thus, water is unlikely to be the cause of the aggregation in the mixtures as the water amount in pure PC is larger than in the mixtures. Note that heating at 150 °C improves the dispersion. However, since the samples are heated in sealed bottles, water cannot escape, therefore the observed changes cannot be attributed to the water content. Instead, these changes could only result from a reorganization of the solid/liquid interface at high temperatures, implying water or not. Although studying the localization of water after separating the NPs from the solvent would be interesting, it falls beyond the scope of this article.

5.3. Clusters

Dispersed stable finite-size clusters are a characteristic of the cobalt ferrite NPs studied here. They exist in all the tested conditions, however their size differs and two levels of clusters seem to exist. To summarize, there are rather large clusters in water, in the initial acidic samples without ligands (see Section 2.1.1) and in aqueous samples with the

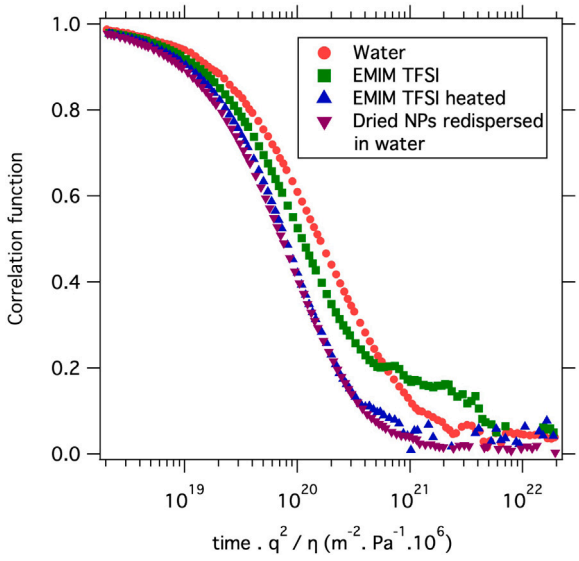

Fig. 6. DLS of dispersions at Φ_{NP} = 1% coated with the ligand $PAC_6MIM^{\pm}$ for APCo2 NPs. Red circle: dispersion in water after the coating with the ligand. Green squares: dispersion after the transfer to EMIM TFSI (no heating). Blue triangles: dispersion in EMIM TFSI after heating at 150 °C; Violet inversed triangles: redispersion in water of coated NPs dried by pumping (see text for details). The *X*-axis is renormalized as in Fig. 5 so that the shifts between the curves only depend on the change of apparent size.

ligands (see Section 4.1, Fig. 4 and Fig. S7). They are then constituted of few dozens of NPs (see Table 2), interacting together through a repulsive force (see Fig. 4). After transfer to EMIM TFSI or PC, these clusters are significantly reduced (see Table 2 and Fig. 5) with low inter-clusters interaction (see Fig. S8). Further heating in these two solvents and their mixtures decreases their size even more, resulting in clusters of only a few NPs (see Table 3).

If heating at 150 °C clearly has some impact in EMIM TFSI and PC, which can result from an interfacial reorganization and/or by the thermal change on the magnetic properties of the NPs, the reduction of aggregation after removing water by pumping is quite unexpected. The influence of the pumping step is therefore also tested in water on the NPs coated with $PAC_6MIM^{\pm}$ ligand. Note that this pumping does not remove all the water: the remaining water is the amount reported for PC in Table 4, and is of the order of one water layer on the NPs' surfaces.

These dried NPs coated with the $PAC_6MIM^{\pm}$ ligand are not only easily redispersable in water but moreover also with much smaller clusters! This is clear from the renormalized DLS (Fig. 6) and from the SAXS measurements (See Fig. S9 in ESI). Both techniques show that this aqueous dispersion of dried NPs and the heated dispersion in the pure IL have rather similar nanostructures.

This low-pressure step can thus remove some component that is neither removed by the washing steps while modifying the surface (see Section 3.1), nor removed by dialysis in acidic medium, also tested. Another option is a breaking of the clusters due to the increase of the ionic strength in the intermediate concentrated states during the drying process. This argument has been mentioned in literature to explain why particles can sometimes be redispersed after drying [43]. However, dispersibility is neither systematic nor easy to predict and some additives are often necessary to enable redispersion. Dispersions post-drying similar to the initial state have been reported but we are not aware of an improvement in the dispersions as evidenced here.

5.4. Ionic liquid-solvent mixtures

In the EMIM TFSI/PC mixtures, the solvent evolves from a polar molecular solvent to a salt, resulting in a medium composed solely of ions. In pure solvents, interparticle interaction is electrostatic with some steric contribution in PC and results from the layering of ions at the solid/solvent interface in EMIM TFSI. Most studies on mixtures in the literature show colloidal aggregation, such as in mixtures of hydrophilic ionic liquids and water [44–47] or hydrophobic ones and water [47]. Recently some of us reported stable iron oxide NPs on the whole range of composition in ethylammonium nitrate (EAN) / water mixtures, showing that the short range organization at the solid–liquid interface can be sufficient to keep the NPs separated [17]. It appears to be the same situation here, meaning that is was not a unique exception.

Here, the interparticle interaction appears to be slightly repulsive on the whole range of compositions of the mixed solvents, within the hypothesis of clusters independent of the concentration, which differs from the case of EAN/water mixtures. The interparticle interaction was indeed slightly attractive in a range of compositions, however no clusters were formed [17].

6. Conclusion

Cobalt ferrites nanoparticles with a maghemite shell synthesized by hydrothermal coprecipitation are successfully dispersed into the ionic liquid EMIM TFSI, the polar solvent propylene carbonate and their binary mixtures.

The water-based dispersions of typical 9 nm diameter NPs are first tested with three different surface ligands, and the behavior of these NPs appears rather different from the one of pure maghemite [24]. First, they are dispersed in water as small clusters of 25–50 NPs, probably due to the higher Hamaker constant for cobalt ferrite compared to maghemite, with some possible contribution of the magnetic interactions for the largest NPs. Such dispersions exhibit repulsive interaction between clusters. Moreover, only the ligands with a phosphonic group enable proper dispersion in EMIM TFSI, with a surface coverage around 2.4 molecules/nm^2 of NP surface.

With the phosphonate $PAC_6MIM^{\pm}Br^{-}$ (1-(6-hexyl phosphonate) 3-methyl imidazolium bromide) as ligand at the NP/solvent interface, stable colloidal dispersions are obtained in EMIM TFSI as well as in pure PC. The mixtures of EMIM TFSI and PC have been characterized: while the viscosity decreases by PC addition in the ionic liquid, the electrical conductivity presents a maximum at $x_{IL} \sim 0.2 - 0.3$, resulting from the balance between viscosity and ion concentration.

Stable colloidal dispersions were achieved for all tested compositions, regardless of the salt concentration. This is noteworthy, as the literature on ionic liquid/solvent mixtures typically reports flocculated dispersions. In contrast, the obtained colloids remain stable for at least several months, as tested with a nanoparticle volume fraction of 1%.

In these non-aqueous solvents, the NPs are dispersed as smaller clusters compared to their dispersion in water, consisting of only a few NPs. This reduction in aggregation is experimentally achieved through a low-pressure pumping step (0.0031 mbar) that removes water and a subsequent heating step at 150 °C. Both steps can modify the organization of the solid/liquid interface in nature and/or in structure, to obtain an equilibrium state that is not attainable at room temperature using the initial synthesis processes. The remaining water molecules appear to be removed from the NPs' surface in the ionic liquid and cannot explain the aggregation in the EMIM TFSI/PC mixtures.

The dispersions at the maximal electrical conductivity are promising candidates as complex liquids for the investigation of thermoelectricity in liquid thermocells. However, it will be necessary to explore the detailed role of several parameters, such as the remaining water content or the interaction with the surface of the thermocell electrode.

CRediT authorship contribution statement

A.A.A. Meireles Guerra: Writing – review & editing, Writing – original draft, Visualization, Validation, Methodology, Investigation, Formal analysis, Conceptualization. **G. Gomide:** Writing – review

& editing, Writing – original draft, Visualization, Validation, Software, Methodology, Investigation, Formal analysis, Conceptualization. **S. Ibrahim:** Methodology, Investigation, Conceptualization. **P. Burckel:** Writing – review & editing, Validation, Investigation, Formal analysis. **P. Coppola:** Methodology, Investigation, Conceptualization. **J. Depeyrot:** Supervision, Project administration, Funding acquisition. **R. Perzynski:** Writing – review & editing, Writing – original draft, Visualization, Validation, Methodology, Investigation, Formal analysis, Conceptualization. **V. Peyre:** Writing – review & editing, Writing – original draft, Visualization, Validation, Methodology, Investigation, Formal analysis, Conceptualization. **S. Papović:** Writing – review & editing, Writing – original draft, Validation, Resources, Methodology, Investigation, Formal analysis. **M. Vraneš:** Writing – review & editing, Writing – original draft, Validation, Resources, Methodology, Investigation, Formal analysis. **E. Dubois:** Writing – review & editing, Writing – original draft, Visualization, Validation, Supervision, Software, Resources, Project administration, Methodology, Investigation, Funding acquisition, Formal analysis, Data curation, Conceptualization. **A.F.C. Campos:** Writing – review & editing, Writing – original draft, Visualization, Validation, Supervision, Project administration, Methodology, Investigation, Formal analysis, Conceptualization.

Declaration of competing interest

The authors declare that they have no known competing financial interests or personal relationships that could have appeared to influence the work reported in this paper.

Data availability

Data will be made available on request.

Acknowledgments

We thank the synchrotron Soleil (France) for beamtime allocation on Swing in the frame of the BAGs projects 20221057 and 20231786. We thank Ana Gabriela Porras Gutierrez and Sandrine Leclerc for the Karl Fisher titrations. We thank Delphine Talbot and Aude Michel for the determinations of metal concentrations by FAAS. We thank for funding the program CAPES-COFECUB Ph 959/20 between France and Brazil, as well as the French program ANR WH-RECOLTE. We are also grateful for the financial support from the Brazilian agencies: the National Council for Scientific and Technological Development (CNPq) grant 303101/2022-9, and the Distrito Federal Research Foundation (FAPDF) grants 0193.001194/2016, 0193.001569/2017, and 0193-00000229/2021-21.

Appendix A. Supplementary data

Supplementary material related to this article can be found online at https://doi.org/10.1016/j.colsurfa.2024.135233.

References

[1] N. Jones, Waste heat: Innovators turn to an overlooked renewable resource, 2018, URL https://e360.yale.edu/features/waste-heat-innovators-turn-to-an-overlooked-renewable-resource.

[2] M. Dupont, D. MacFarlane, J. Pringle, Thermo-electrochemical cells for waste heat harvesting— progress and perspectives, Chem. Commun. 53 (2017) 6288–6302, http://dx.doi.org/10.1039/c7cc02160g.

[3] A. Würger, Transport in charged colloids driven by thermoelectricity, Phys. Rev. Lett. 101 (2008) 108302, http://dx.doi.org/10.1103/PhysRevLett.101.108302.

[4] A. Majee, A. Würger, Collective thermoelectrophoresis of charged colloids, Phys. Rev. E 83 (2011) 061403, http://dx.doi.org/10.1103/PhysRevE.83.061403.

[5] I. Nkurikiyimfura, Y. Wang, Z. Pan, Heat transfer enhancement by magnetic nanofluids—A review, Renew. Sustain. Energy Rev. 21 (2013) 548–561, http://dx.doi.org/10.1016/j.rser.2012.12.039.

[6] T.J. Salez, M. Kouyaté, C. Filomeno, M. Bonetti, M. Roger, G. Demouchy, E. Dubois, R. Perzynski, A. Cebers, S. Nakamae, Magnetically enhancing the seebeck coefficient in ferrofluids, Nanoscale Adv. 1 (2019) 2979–2989, http://dx.doi.org/10.1039/c9na00109c.

[7] T.J. Salez, B.T. Huang, M. Rietjens, M. Bonetti, C. Wiertel-Gasquet, M. Roger, C.L. Filomeno, E. Dubois, R. Perzynski, S. Nakamae, Can charged colloidal particles increase the thermoelectric energy conversion efficiency? Phys. Chem. Chem. Phys. 19 (2017) 9409–9416, http://dx.doi.org/10.1039/C7CP01023K.

[8] M. Bonetti, S. Nakamae, M. Roger, G. P., Huge seebeck coefficients in nonaqueous electrolytes, J. Chem. Phys. 134 (2011) 114513, http://dx.doi.org/10.1063/1.3561735, 1–8.

[9] E. Laux, S. Uhl, L. Jeandupeux, P. Lopez, S. P., E. Vanoli, R. Marti, H. Knepper, Thermoelectric generators based on ionic liquids, J. Electron. Mater. 47 (2018) 3193–3197, http://dx.doi.org/10.1007/s11664-018-6175-z.

[10] A. Tiozzo, A. Bertinetti, A. Tommasi, G. Nicol, R. Rocca, S. Nakamae, B. Torres Bautista, S. Campagna Zignani, E. Laux, S. Fantini, S. M.F., From academia to industry: Criteria for upscaling ionic liquid-based thermo- electrochemical cells for large-scale applications, Energies 17 (2024) 1 1–12, http://dx.doi.org/10.3390/en17010001.

[11] B.D. Prince, P. Tiruppathi, R.J. Bemish, Y.-H. Chiu, E.J. Maginn, Molecular dynamics simulations of 1-ethyl-3-methylimidazolium bis [(trifluoromethyl) sulfonyl] imide clusters and nanodrops, J. Phys. Chem. A 119 (2) (2015) 352–368, http://dx.doi.org/10.1021/jp507073e.

[12] S. Werner, M. Haumann, P. Wasserscheid, Ionic liquids in chemical engineering, Annu. Rev. Chem. Biomol. Eng. 1 (Volume 1, 2010) (2010) 203–230, http://dx.doi.org/10.1146/annurev-chembioeng-073009-100915, URL https://www.annualreviews.org/content/journals/10.1146/annurev-chembioeng-073009-100915.

[13] N.R. Levy, S. Lifshits, E. Yohanan, Y. Ein-Eli, Hybrid ionic liquid propylene carbonate-based electrolytes for aluminum–air batteries, ACS Appl. Energy Mater. 3 (3) (2020) 2585–2592, http://dx.doi.org/10.1021/acsaem.9b02288.

[14] P.H. Lam, A.T. Tran, D.J. Walczyk, A.M. Miller, L. Yu, Conductivity, viscosity, and thermodynamic properties of propylene carbonate solutions in ionic liquids, J. Mol. Liq. 246 (2017) 215–220, http://dx.doi.org/10.1016/j.molliq.2017.09.070.

[15] J.C. Riedl, M.A. Akhavan Kazemi, F. Cousin, E. Dubois, S. Fantini, S. Loïs, R. Perzynski, V. Peyre, Colloidal dispersions of oxide nanoparticles in ionic liquids: elucidating the key parameters, Nanoscale Adv. 2 (2020) 1560–1572, http://dx.doi.org/10.1039/C9NA00564A.

[16] T. Fiuza, M. Sarkar, J.C. Riedl, M. Beaughon, B.E. Torres Bautista, K. Bhattacharya, F. Cousin, E. Barruet, G. Demouchy, J. Depeyrot, E. Dubois, F. Gélébart, V. Geertsen, G. Mériguet, L. Michot, S. Nakamae, R. Perzynski, V. Peyre, Ion specific tuning of nanoparticle dispersion in an ionic liquid: a structural, thermoelectric and thermo-diffusive investigation, Phys. Chem. Chem. Phys. 25 (42) (2023) 28911–28924, http://dx.doi.org/10.1039/D3CP02399K, URL http://xlink.rsc.org/?DOI=D3CP02399K.

[17] T. Fiuza, M. Sarkar, J.C. Riedl, F. Cousin, G. Demouchy, J. Depeyrot, E. Dubois, R. Perzynski, V. Peyre, Dispersions of magnetic nanoparticles in water/ ionic liquid mixtures, Faraday Discuss. (2024) http://dx.doi.org/10.1039/D4FD00028E, URL http://dx.doi.org/10.1039/D4FD00028E.

[18] M. Vasilakaki, I. Chikina, V. Shikin, N. Ntallis, D. Peddis, A. Varlamov, K. Trohidou, Towards high-performance electrochemical thermal energy harvester based on ferrofluids, Appl. Mater. Today 19 (2020) 100587, http://dx.doi.org/10.1016/j.apmt.2020.100587, URL https://cea.hal.science/cea-03747392.

[19] M. Vasilakaki, J. Chikina, V. Shikin, N. Ntallis, D. Peddis, A. Varlamov, K. Trohidou, Enhancement of the seebeck coefficient in ferrofluid based thermoelectric materials: A numerical study, Mater. Today: Proc. 44 (2021) 3483–3488, http://dx.doi.org/10.1016/j.matpr.2020.05.811, 17th European Thermoelectric Conference URL https://www.sciencedirect.com/science/article/pii/S2214785320344242.

[20] J.D.A. Gomes, M.H. Sousa, F.A. Tourinho, R. Aquino, G.J.D. Silva, J. Depeyrot, E. Dubois, R. Perzynski, Synthesis of core-shell ferrite nanoparticles for ferrofluids: Chemical and magnetic analysis, J. Phys. Chem. C 112 (2008) 6220–6227, http://dx.doi.org/10.1021/jp7097608.

[21] R. Aquino, F.A. Tourinho, R. Itri, M.C.F.L. e Lara, J. Depeyrot, Size control of MnFe2O4 nanoparticles in electric double layered magnetic fluid synthesis, J. Magn. Magn. Mater. 252 (2002) 23–25, http://dx.doi.org/10.1016/S0304-8853(02)00607-8.

[22] A.F.C. Campos, R. Aquino, F.A. Tourinho, F.L.O. Paula, J. Depeyrot, Influence of the spatial confinement at nanoscale on the structural surface charging in magnetic nanocolloids, Eur. Phys. J. E 36 (2013) 42, http://dx.doi.org/10.1140/epje/i2013-13042-y.

[23] G. Meriguet, E. Wandersman, E. Dubois, A. Cebers, J. Gomes, G. Demouchy, J. Depeyrot, A. Robert, R. Perzynski, Magnetic fluids with tunable interparticle interaction: Monitoring under-field local structure, Magnetohydrodynamics 48 (2) (2012) 415–425, http://dx.doi.org/10.22364/mhd.

[24] J.C. Riedl, M. Sarkar, T. Fiuza, F. Cousin, J. Depeyrot, E. Dubois, G. Mériguet, R. Perzynski, V. Peyre, Design of concentrated colloidal dispersions of iron oxide nanoparticles in ionic liquids: Structure and thermal stability from 25 to 200 c, J. Colloid Interface Sci. 607 (2022) 584–594, http://dx.doi.org/10.1016/j.jcis.2021.08.017.

[25] P.A. Hunt, Why does a reduction in hydrogen bonding lead to an increase in viscosity for the 1-butyl-2, 3-dimethyl-imidazolium-based ionic liquids? J. Phys. Chem. B 111 (18) (2007) 4844–4853, http://dx.doi.org/10.1021/jp067182p.
[26] M. Vraneš, N. Zec, A. Tot, S. Papović, S. Dožić, S. Gadžurić, Density, electrical conductivity, viscosity and excess properties of 1-butyl-3-methylimidazolium bis (trifluoromethylsulfonyl) imide+ propylene carbonate binary mixtures, J. Chem. Thermodyn. 68 (2014) 98–108, http://dx.doi.org/10.1016/j.jct.2013.08.034.
[27] A. Hofmann, M. Migeot, T. Hanemann, Investigation of binary mixtures containing 1-ethyl-3-methylimidazolium bis (trifluoromethanesulfonyl) azanide and ethylene carbonate, J. Chem. Eng. Data 61 (1) (2016) 114–123, http://dx.doi.org/10.1021/acs.jced.5b00338.
[28] J. Papan Djaniš, G.G. Princič, A. Mavrič, A. Mertelj, J. Iskra, D. Lisjak, New insights into amino-functionalization of magnetic nanoplatelets with silanes and phosphonates, Nanomaterials 12 (12) (2022) 2123, http://dx.doi.org/10.3390/nano12122123.
[29] R. Weerasooriya, H. Wickramarathna, Modeling anion adsorption on kaolinite, J. Colloid Interface Sci. 213 (2) (1999) 395–399, http://dx.doi.org/10.1006/jcis.1999.6103.
[30] D. Lisjak, P. Hribar Bostjancic, A. Mertelj, A. Mavric, M. Valant, J. Kovac, H. Hudelja, A. Kocjan, D. Makovec, Formation of fe (III)-phosphonate coatings on barium hexaferrite nanoplatelets for porous nanomagnets, ACS omega 5 (23) (2020) 14086–14095, http://dx.doi.org/10.1021/acsomega.0c01597.
[31] B. Frka-Petesic, E. Dubois, L. Almasy, V. Dupuis, F. Cousin, R. Perzynski, Structural probing of clusters and gels of self-aggregated magnetic nanoparticles, Magnetohydrodynamics 49 (3–4) (2013) 328–338, http://dx.doi.org/10.22364/mhd.49.3-4.15.
[32] M. Lin, H. Lindsay, D. Weitz, R. Ball, R. Klein, P. Meakin, Universal reaction-limited colloid aggregation, Phys. Rev. A 41 (1990) 2005–2020, http://dx.doi.org/10.1103/PhysRevA.41.2005.
[33] E. Novak, E. Pyanzina, P. Sanchez, S. Kantorovich, The structure of clusters formed by stockmayer supracolloidal magnetic polymers, Eur. Phys. J. E 42 (2019) 158 1–9, http://dx.doi.org/10.1140/epje/i2019-11924-6.
[34] M. Mamusa, J. Sirieix-Plénet, R. Perzynski, F. Cousin, E. Dubois, V. Peyre, Concentrated assemblies of magnetic nanoparticles in ionic liquids, Faraday Discuss. 181 (2015) 193–209, http://dx.doi.org/10.1039/C5FD00019J.
[35] M. Metzger, B. Strehle, S. Solchenbach, H.A. Gasteiger, Hydrolysis of Ethylene Carbonate with Water and Hydroxide under Battery Operating Conditions, J. Electrochem. Soc. 163 (7) (2016) A1219–A1225, http://dx.doi.org/10.1149/2.0411607jes, URL https://iopscience.iop.org/article/10.1149/2.0411607jes.
[36] J. Riedl, Dispersions of nanomagnets in ionic liquids for thermoelectric applications (Ph.D. thesis), Sorbonne Universite, 2020.
[37] M.B. Fernández van Raap, P. Mendoza Zélis, D. Coral, T. Torres, C. Marquina, G.F. Goya, F.H. Sánchez, Self organization in oleic acid-coated CoFe2o4 colloids: a saxs study, J. Nanoparticle Res. 14 (2012) 1–10, http://dx.doi.org/10.1007/s11051-012-1072-5.
[38] W.B. Goodwin, D. Shin, D. Sabo, S. Hwang, Z.J. Zhang, J.C. Meredith, K.H. Sandhage, Tunable multimodal adhesion of 3D, nanocrystalline CoFe2O4 pollen replicas, Bioinspiration & biomimetics 12 (6) (2017) 066009, http://dx.doi.org/10.1088/1748-3190/aa7c89.
[39] B. Faure, G. Salazar-Alvarez, L. Bergstrom, Hamaker constants of iron oxide nanoparticles, Langmuir 27 (14) (2011) 8659–8664, http://dx.doi.org/10.1021/la201387d.
[40] S.P. Pujari, L. Scheres, A.T.M. Marcelis, H. Zuilhof, Covalent Surface Modification of Oxide Surfaces, Angewandte Chemie International Edition 53 (25) (2014) 6322–6356, http://dx.doi.org/10.1002/anie.201306709, URL https://onlinelibrary.wiley.com/doi/10.1002/anie.201306709.
[41] N.F. Catherall, A.G. Williamson, Mutual solubilities of propylene carbonate and water, J. Chem. Eng. Data 16 (3) (1971) 335–336, http://dx.doi.org/10.1021/je60050a021, URL https://pubs.acs.org/doi/abs/10.1021/je60050a021.
[42] M. Han, R.M. Espinosa-Marzal, Influence of Water on Structure, Dynamics, and Electrostatics of Hydrophilic and Hydrophobic Ionic Liquids in Charged and Hydrophilic Confinement between Mica Surfaces, ACS Appl. Mater. Interfaces 11 (36) (2019) 33465–33477, http://dx.doi.org/10.1021/acsami.9b10923, URL https://pubs.acs.org/doi/10.1021/acsami.9b10923.
[43] S. Shrestha, B. Wang, P. Dutta, Nanoparticle processing: Understanding and controlling aggregation, Adv. Colloid Interface Sci. 279 (2020) 102162, http://dx.doi.org/10.1016/j.cis.2020.102162, URL https://linkinghub.elsevier.com/retrieve/pii/S0001868619304816.
[44] I. Szilagyi, T. Szabo, A. Desert, G. Trefalt, T. Oncsik, M. Borkovec, Particle aggregation mechanisms in ionic liquids, Phys. Chem. Chem. Phys. 16 (20) (2014) 9515–9524, http://dx.doi.org/10.1039/C4CP00804A, URL http://xlink.rsc.org/?DOI=C4CP00804A.
[45] J.A. Smith, O. Werzer, G.B. Webber, G.G. Warr, R. Atkin, Surprising Particle Stability and Rapid Sedimentation Rates in an Ionic Liquid, J. Phys. Chem. Lett. 1 (1) (2010) 64–68, http://dx.doi.org/10.1021/jz9000642, URL http://pubs.acs.org/doi/10.1021/jz9000642.
[46] D. Takacs, M. Tomsic, I. Szilagyi, Effect of water and salt on the colloidal stability of latex particles in ionic liquids soltions, Colloids Interfaces 6 (2022) 2–14, http://dx.doi.org/10.3390/colloids6010002.
[47] K. Sakai, K. Okada, A. Uka, T. Misono, T. Endo, S. Sasaki, M. Abe, H. Sakai, Effects of Water on Solvation Layers of Imidazolium-Type Room Temperature Ionic Liquids on Silica and Mica, Langmuir 31 (22) (2015) 6085–6091, http://dx.doi.org/10.1021/acs.langmuir.5b01184, URL https://pubs.acs.org/doi/10.1021/acs.langmuir.5b01184.